Pure appl. geophys. 161 (2004) 2451–2463
0033–4553/04/122451–13
DOI 10.1007/s00024-004-2575-5



Pure and Applied Geophysics

# Emergent Anisotropy and Flow Alignment in Viscous Rock

H.-B. MÜHLHAUS[1, 2], L. MORESI[3], and M. ČADA[4]

*Abstract*—A novel class of nonlinear, visco-elastic rheologies has recently been developed by MÜHLHAUS *et al.* (2002a, b). The theory was originally developed for the simulation of large deformation processes including folding and kinking in multi-layered visco-elastic rock . The orientation of the layer surfaces or slip planes in the context of crystallographic slip is determined by the normal vector the so-called director of these surfaces. Here the model (MÜHLHAUS *et al.*, 2002a, b) is generalized to include thermal effects; it is shown that in 2-D steady states the director is given by the gradient of the flow potential. The model is applied to anisotropic simple shear where the directors are initially parallel to the shear direction. The relative effects of textural hardening and thermal softening are demonstrated. We then turn to natural convection and compare the time evolution and approximately steady states of isotropic and anisotropic convection for a Rayleigh number $Ra = 5.64 \times 10^5$ for aspect ratios of the experimental domain of 1 and 2, respectively. The isotropic case has a simple steady-state solution, whereas in the orthotropic convection model patterns evolve continuously in the core of the convection cell, which makes only a near-steady condition possible. This near-steady state condition shows well aligned boundary layers, and the number of convection cells which develop appears to be reduced in the orthotropic case. At the moderate Rayleigh numbers explored here we found only minor influences in the change from aspect ratio one to two in the model domain.

## *Introduction*

During the past decade, geoscientists have come to appreciate the often-powerful role played by computer simulations as a tool to enhance our understanding of geological processes. While early simulations were often based on rheologies and computer packages from the engineering world, there is an increasing awareness that these methods are only suited for a limited number of geological problems. An obvious example is the study of finite strain viscoelasticity with strongly history-dependent material behavior, where most engineering codes are optimized to study the modest strains which accumulate prior to failure. Computer models must be

[1] The University of Queensland, St. Lucia, QLD 4072, Australia.
E-mail: muhlhaus@quakes.uq.edu.au
[2] CSIRO Division of Exploration and Mining, 26 Dick Perry Ave., Kensington WA 6051, Australia.
[3] School of Mathematical Sciences, Monash University, PO Box 28M, Clayton, Victoria 3800, Australia. E-mail: louis.moresi@msci.monash.edu.au
[4] Ludwig-Maximilians University, Institute of Geophysics, Theresienstr. 41, 80333 Munich, Germany. E-mail: miro.cada@addcom.de

constrained by observational data. In the case of studies of the Earth's interior, analysis of seismic observations has provided the principal information. In particular, seismic tomography is yielding ever improved estimates of seismic wave velocities and anisotropy which can be interpreted as a filtered snapshot of density and instantaneous flow patterns. There is, however, no time information on mantle flow in the seismic data so the emergence of plate tectonics and material anisotropy must be deduced from other means. Computer simulations of these phenomena can in principle provide such a means. However a numerical simulation model for mantle convection and the emergence of plate tectonics, which simulates the development of anisotropic texture of the lithosphere and mantle, is a difficult modelling exercise, requiring a sophisticated mix of developments of constitutive relationships and of numerical methodology. In this context, the seismic tomography derived anisotropy models of the earth (e.g., DEBAYLE and KENNETT, 2000) represent an important constraint on present-day flow patterns. The emergent anisotropy predicted in numerical simulations would improve interpretation of seismic tomography derived anisotropy models in terms of flow patterns and their evolution.

The direct simulation of anisotropic mantle flow has been a very specialized area with very few publications since the original paper of CHRISTENSEN (1987). In general it has instead been assumed that the instantaneous flow patterns predicted by convection simulations can be mapped immediately to seismic anisotropy. However, the results of SIMONS *et al.,* (2002) and many others show the observations to be far more advanced than this simplistic modeling assumption. Recent work by Parmentier and coworkers (FISCHER *et al.*, 2000; FOUCH *et al.*, 1997) is considerably more sophisticated, but does not treat the director as a distinct internal material variable. Advanced models should include feedback processes between large-scale flow, director misalignment and the drive towards flow alignment. A step in this direction in the context of folding was described by MÜHLHAUS *et al.*, (2002a, b). The present paper represents a continuation of this work; the rheology is refined to include temperature-dependent parameters. The performance of the model is illustrated in finite-element simulations of anisotropic simple shear and anisotropic natural convection. Furthermore we present an outlook on a more appropriate anisotropy model that will be implemented in the future models.

## *Specific viscous and visco-elastic constitutive relations*

Layered material is not only ubiquitous in geological formations of the crust, but seems to be likely even in deeper regions. The existence of a low viscosity zone around the seismic low velocity zone had been proposed as a result of post glacial rebound studies. This zone was suggested to consist of soft layers (Cathles, 1975). In the late sixties laminated mantle models were proposed by different authors in order to explain the discrepancies of Love and Rayleigh wave dispersion (AKI, 1968;

TAKEUCHI *et al.*, 1968). Recent post glacial rebound studies (SPADA *et al.* 1991) suggest seismic observation data around deglaciated regions such as the passive margins of Fennoscandia, may help to constrain lower mantle viscosity, and in fact indicate a highly viscous lower mantle. On the other hand recent experimental studies on garnet (KARATO *et al.*, 1995) and on wadsleyite (YOUNG *et al.*, 1993) have lead to two different views on the viscosity of the transition zone. If garnet is the dominant mineral in the transition zone, this zone then could be a layer of increased viscosity. In the event that the transformation from hydrous olivine to wandsleyite during subduction releases water into deeper zones, the viscosity in the transition zone would decrease. It is obvious that the viscosity stratification is a wildly discussed and not well understood detail, although at least a stratification is an accepted model.

We consider in both models (-in the simple shear and the convection study-) a locally transverse-isotropic, viscous material. The transverse-isotropy may represent an alternating sequence of hard and soft materials or a superposition of layers of one material weakly bonded along their interfaces. Another possible contribution to anisotropy is preferred orientation of crystallographic slip planes. Acoustic wave anisotropy in seismology is consistent with the anisotropy of the constituent minerals and especially their slip plane orientation.

Two classes of anisotropic structures are thought to cause seismic anisotropy in the Earth's mantle. One is the lattice preferred orientation of anisotropic minerals and the other is the shape preferred orientation of secondary phases (KARATO 1998). The orientation is characterized by a director which, in the case of a layered material or a material with preferred crystallographic slip, is oriented normal to the layer or slip surface, respectively. The term ''director'' is adopted from the physics of liquid crystals (de Gennes and Prost [6]). Transverse-isotropic relations are characterized by two effective viscosities. We designate the normal viscosity as $\eta$ and the shear viscosity as $\eta_S$ so that if the coordinate axes are chosen locally aligned with the axes of anisotropy then $\sigma_{11} - \sigma_{22} = 4\eta D_{11}$, $\sigma_{12} = 2\eta_S D_{12}$ and $D_{11} = -D_{22}$ where $\sigma_{ij}$ designate the Cartesian components of the stress tensor and $D_{ij}$ is the stretching.

In the following simple model for a layered viscous material we correct the isotropic part $2\eta D'_{ij}$ of the model by means of the $\Lambda_{ijkl}$ tensor (MÜHLHAUS *et al.*, 2002a, b) to consider the mechanical effect of the layering; thus

$$\sigma_{ij} = 2\eta D'_{ij} - 2(\eta - \eta_S)\Lambda_{ijkl} D'_{kl} - p\delta_{ij}, \tag{1}$$

where a prime designates the deviator of the respective quantity, $p$ is the pressure, $D_{ij}$ is the stretching, $\sigma_{ij}$ is the Cauchy or true stress and

$$\Lambda_{ijkl} = \frac{1}{2}(n_i n_k \delta_{lj} + n_j n_k \delta_{il} + n_i n_l \delta_{kj} + n_j n_l \delta_{ik}) - 2n_i n_j n_k n_l. \tag{2}$$

In (1) and (2) the vector $n_i$ is the unit orientation vector of the director $N_i$. The orientation of the normal vector or director changes with deformation. In order to track the fabric development (e.g. LPO) with time, we have to derive a relation

between the present deformation field and the orientation of the director. We must obtain an evolution equation which enables us to understand the time history of the slip planes.

In the present applications we assume that the director transforms as a material surface element. In continuum mechanics theory the evolution of the director of the layers is described by the Nanson relation (Belytschko *et al.*, 2001):

$$N_i dA = \mathcal{J} N_j^0 (F_{ij}^{-1})^T dA_0 \text{ with } \mathcal{J} = \det \mathbf{F} \text{ and } F_{ij} \equiv \frac{\partial x_i}{\partial X_j}. \tag{3}$$

$\mathcal{J}$ is the Jacobian matrix and $\mathbf{F}$ is the deformation gradient. This relation relates the current normal vector (the director) to the reference normal vector (Belytschko *et al.*, 2001).

$$\dot{N}_i = -L_{ji} N_j \text{ where } L_{ij} = v_{i,j}. \tag{4}$$

Inserting the definition of the material derivative on the left-hand side, (4) may be written as:

$$N_{i,t} + v_j N_{i,j} = -v_{j,i} N_j, \tag{5}$$

where $v_i$ is the velocity vector. For steady states the partial time derivative vanishes and (5) may be re-written as:

$$v_j (N_{i,j} - N_{j,i}) = -(v_j N_j)_{,i}. \tag{6}$$

In 2-D it is plausible that the planes of anisotropy or slip planes are aligned with the velocity vectors in steady states, which is equivalent to normality of the directors to the velocity vectors. If normality holds then the right-hand side of (6) vanishes since $|\mathbf{v}||\mathbf{N}| \cos(\pi/2)$. A perfectly flow-aligned steady-state solution exists if the left-hand side vanishes as well. To show this we write the left-hand side in components and remember that for the description of an incompressible flow the stream function $\Psi$ can be introduced:

$$v_{i,i} = v_{1,1} + v_{2,2} = \Psi_{,12} - \Psi_{,21} = 0. \tag{7}$$

The gradient of the potential is orthogonal to the velocity field, i.e., $N_i = \Psi_{,i}$ and hence we can write the left-hand side:

$$v_1 (N_{2,1} - N_{1,2}) + v_2 (N_{1,2} - N_{2,1}) = \Psi_{,2} (\Psi_{,21} - \Psi_{,12}) + \Psi_{,1} (\Psi_{,12} - \Psi_{,21}) = 0. \tag{8}$$

In this particular case the director orientation need not be included explicitly as an independent variable, which simplifies the formulation considerably.

### *Crystallographic slip*

In the convection simulations presented in next to last section of this paper we restrict ourselves to constant viscosities for simplicity. This is of course a very coarse

simplification if crystallographic slip is the main mechanism. Because of the importance of this issue we briefly outline here how power-law behavior can be incorporated into the present model without changing the tensor structure of the constitutive relations.

In general the shear stress on the slip plane with unit normal **n** is defined as:

$$\tau^N = \sqrt{\sigma_{ij}\Lambda_{ijkl}\sigma_{kl}} \tag{9}$$

where $\Lambda_{ijkl}$ is the 4th order tensor (2) in our anisotropic stress-stretching relationship; we use the superscribed $N$ instead of $n$ to designate the shear stress on the $N$-slip plane to avoid confusion with the power-law index as used below. In 2-D there is a simpler way to calculate $\tau^N$: The stress vector on the $N$slip surface is:

$$t_i = \sigma_{ij}n_j. \tag{10}$$

Let **m** be a vector in the slip plane so that $\mathbf{m}\cdot\mathbf{n} = 0$. In 2-D the components of **m** read:

$$\mathbf{m} = \begin{pmatrix} n_2 \\ -n_1 \end{pmatrix}. \tag{11}$$

The magnitude of the shear stress on the $n$-surface is then defined as:

$$\tau^N = |\sigma_{ij}n_jm_i| = |n_1n_2(\sigma_{11} - \sigma_{22}) + \sigma_{12}(n_2^2 - n_1^2)|. \tag{12}$$

We formulate our constitutive relationship with respect to the (**m**, **n**) coordinate system for convenience. We have:

$$D_{nm} = [D_{nm}]_{Newt} + [D_{nm}]_{pow}. \tag{13}$$

The subscript *Newt* and *pow* in (13) stand for linear viscous and power law. For the viscous term we have:

$$[D_{nm}]_{Newt} = \frac{1}{2\eta}\sigma_{nm}, \tag{14}$$

where $\tau^N = |\sigma_{nm}|$ where $\sigma_{nm} = n_1n_2(\sigma_{11} - \sigma_{22}) + \sigma_{12}(n_2^2 - n_1^2)$. The power-law term is defined as:

$$[D_{nm}]_{pow} = \left(\frac{\dot{\gamma}^Y}{\tau_Y^N}\left(\frac{\tau^N}{\tau_Y^N}\right)^{n-1}\right)\sigma_{nm}. \tag{15}$$

We define:

$$\frac{1}{\eta_{pow}} \equiv \left(\frac{\dot{\gamma}_Y}{\tau_Y^N}\left(\frac{\tau^N}{\tau_Y^N}\right)^{n-1}\right). \tag{16}$$

Note that the power-law contribution to the total shear strain rate $D_{nm}$ is small if the power-law exponent $n \gg 1$ and the yield shear stress $\tau_Y^N \gg \tau^N$. In equation (15) and

(16) $\dot{\gamma}_Y$ is a reference strain rate. In the present context the shear viscosity $\eta_S$ is obtained as:

$$\frac{1}{2\eta_S} = \frac{1}{2\eta} + \frac{1}{2\eta_{pow}} = \frac{1}{2\eta} + \frac{1}{2}\left(\frac{\dot{\gamma}_Y}{\tau_Y^N}\left(\frac{\tau^N}{\tau_Y^g}\right)^{n-1}\right) \tag{17}$$

and hence:

$$\eta_s = \frac{\eta}{1 + \eta \frac{\dot{\gamma}_Y (\tau^N)^{n-1}}{(\tau_Y)^n}}. \tag{18}$$

It is obvious that in (18) the shear viscosity $\eta_S$ equals $\eta$ for $\tau_Y^N \gg \tau^N$ and $n \gg 1$, i.e., isotropy. The shear viscosity $\eta_S$ is expressed in terms of $\eta$ and three new parameters: the power law exponent $n$, and the reference or yield stress and strain rate $\tau_Y^N$ and $\dot{\gamma}_Y$, respectively.

The values for $\eta_S$ range between 0 and $\eta$ where the extreme values can only be reached if the power-law exponent $n$ is infinite (viscous/ideal-plastic behavior).

The situation in the mantle is certainly more complicated than the picture presented to date. Global mantle tomography has revealed that the strength of anisotropy is significantly smaller in the lower mantle region, below a depth of about 300 km. It has also been shown that in particular only the $D''$ layer and presumably the topmost lower mantle region, the transition zone, have significant seismic anisotropy (MONTAGNER and KENNETT, 1996). This is connected with the changing creep processes and therefore also connected with grain sizes and stresses. Plastic

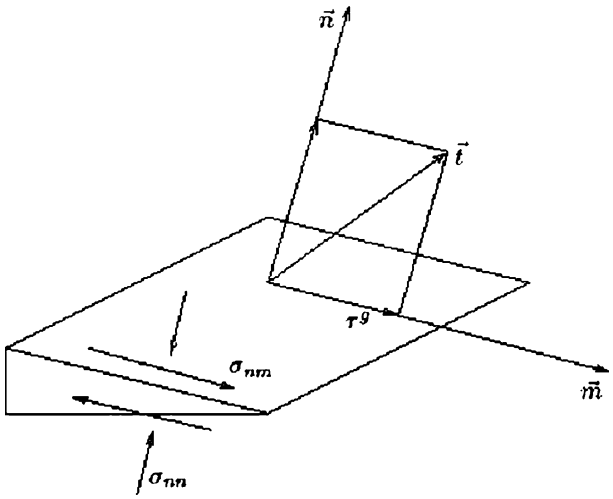


Figure 1
Stress, the normal component, and the stress tensor components acting on a slip surface of a material prism.

flow induces preferred orientations in rock-forming minerals and NICHOLAS and CHRISTENSEN (1987) have shown that homogeneous deformation of a dominant slip system and the orientation of slip directions tend to coincide with the flow direction. Nevertheless grain rotation and also recrystallization in the presence of a thermal gradient can cause preferred orientation and therefore seismic anisotropy. The key requirement in introducing more complicated effects is to include an independent director evolution equation which is possible in our formulation.

### *Simple Shear*

We consider a semi-infinite layer parallel to $x_1$ of thickness $h$. At $x_2 = h$ we apply the constant shear stress $\tau^N$; also at $x_2 = h$ we assume that the temperature is kept constant and $v_2 = 0$. At $x_2 = 0$ we assume that the velocities and the thermal gradient vanishes. At time $t = 0$ the directors are assumed parallel to $x_1$, i.e., the layering is initially orthogonal to the surface of the shear layer. We have considered two cases, namely simple shear with and without temperature dependence ($\sim \exp Q/RT$) of the viscosity. In both calculations we assume that $\eta/\eta_S = 10$.

Analytical solutions for benchmarking isothermal, simple orthotropic shear are easily derived from the relations in the appendix of Mülhaus *et al.* (2002a).

In Figure (2), $V_{\max}$ is the shear velocity at $x_2 = h$ and $T_{\max}$ is the temperature at $x_2 = 0$. The velocity $V_{max}$ drops from 10 to 1 at $\Delta = 1$ where the directors have rotated by $\pi/4$, where $\Delta$ is the displacement of the top layer. For temperature-dependent viscosity the textural hardening is counteracted by thermal softening; i.e., $V_{\max}$ levels out and subsequently increases again after a director rotation of approximately $\pi/4$. The normal strain rates depend on the normal stress and the shear stress in anisotropic simple shear; hence the coupling between the shear stress and the normal stress $\sigma_{22}/\sigma_{12}$ in Figure (2).

### *Anisotropic vs. Isotropic Convection*

We consider standard basally heated convection in a box with aspect ratios of $1 \times 1$ and a $2 \times 1$. On all boundaries we assume that the normal velocities are zero; on the top and bottom boundaries the temperature is kept fixed and on the sides the thermal gradient vanishes. We have a simple linear temperature gradient. In each case we assume a Rayleigh-number of $Ra = 5.64 \times 10^5$ and an anisotropy factor $\eta/\eta_S = 10$. In the definition of the Rayleigh number for anisotropic viscous materials we follow CHRISTENSEN (1987) and define:

$$Ra = \frac{2\alpha\rho_0 g\Delta T H^3}{\kappa(\eta + \eta_S)}, \tag{19}$$

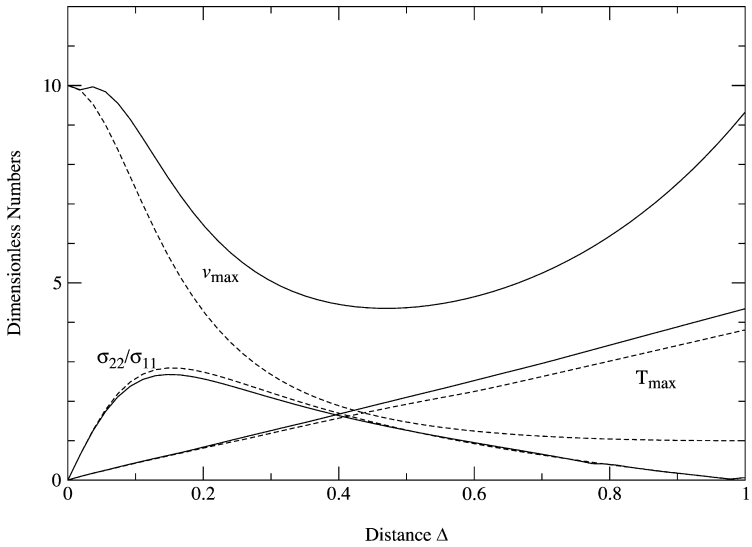


Figure 2
Simple shear of a layer of constant thickness $h$. The details of the boundary conditions are described in the text above. Constant viscosity simulations: broken line; temperature-dependent viscosity: solid line. $Pe = 8400$ (i.e., thermal diffusion is unimportant) and $Di = 0.9$. The dissipation number $Di$ is the coefficient of the shear heating term in the dimensionless heat equation and $\mathrm{Pe}^{-1}$ is the dimensionless thermal diffusion coefficient.

where $\rho_0$ is the density of the cold boundary, $\alpha$ is the thermal expansion coefficient, $\kappa$ is the thermal diffusivity and $H$ is the thickness of the convecting layer. The global characteristics represented in Figure (3) are the root-mean-square of the nodal point velocities $V_{\mathrm{rms}}$ and the Nusselt number, which in 2-D for a box of aspect ratio $L/H$ with zero normal velocities across the box surfaces and fixed temperature differences between the cold and the hot boundary is defined as:

$$Nu = 1 - \frac{H}{L}\int_{-L/2}^{L/2}\frac{1}{2}\left(\widetilde{T}_{,2}\left(x_1, \frac{1}{2}\right) + \widetilde{T}_{,2}\left(x_1, -\frac{1}{2}\right)\right)dx_1, \tag{20}$$

where $\widetilde{T}$ is the convective temperature. Equation (20) is simply a convenient form of the usual definintion of the steady state Nusselt number, i.e., the average total heat flux across the convection box divided by the average flux by conduction only. It simply follows from elementary transformations and application of the Gauss' theorem.

*Numerical method*

Our particle-in-cell finite-element method is based closely on the standard finite element method, and is a derivative of the material point method of SULSKY *et al.* (1995). The standard mesh is used to discretize the domain into elements, and the

shape functions interpolate nodal point values in the mesh in the usual fashion. The problem is formulated in a weak form to give an integral equation, and the shape function expansion produces a discrete (matrix) equation. The stress balance equation in weak form reads:

$$\int_\Omega N_{i,j}\tau_{ij}d\Omega - \int_\Omega N_{,i}pd\Omega = \int_\Omega N_i f_i d\Omega, \tag{21}$$

where the trial functions, $N$, are the shape functions defined by the mesh, and we have assumed that no non-zero traction boundary conditions are present. For the discretized problem, these integrals occur over subdomains (elements) and are calculated by summation over a finite number of sample points within each element. For example, in order to integrate a quantity, $\phi$ over the element domain $\Omega^e$ we replace the continuous integral by a summation

$$\int_{\Omega^e} \phi d\Omega \leftarrow \sum_p w_p \phi(\mathbf{x}_p). \tag{22}$$

In standard finite elements, the positions of the sample points, $\mathbf{x}_p$, and the weighting, $w_p$ are optimized in advance. In our scheme the $\mathbf{x}_p$'s correspond precisely to the Lagrangian points embedded in the fluid, and $w_p$ must be recalculated at the end of a timestep for the new configuration of particles. Constraints on the values of $w_p$ derive from the need to integrate polynomials of a minimum degree related to the degree of the shape function interpolation, and the order of the underlying differential equation (e.g., HUGHES (1984)).

The Lagrangian points carry the history variables (in this case director orientation) which are therefore directly available for the element integrals without the need to interpolate from nodal points to fixed integration points.

## *Convection Patterns*

We have conducted simulations in convection cells of aspect ratio 1 and 2. In the square cell, anisotropic convection concentrates around the cell boundaries encircling a more or less stagnant core. The simulations are based on $32 \times 32$, $64 \times 64$, $64 \times 48$ and $80 \times 48$ square meshes of bilinear quadrilateral elements in the first box of aspect ratio 1 and in the second box of aspect ratio 2, respectively. The wavenumber of the temperature disturbance is $1/\pi$. The momentum, heat and director equations are solved sequentially. Advection terms do not appear explicitly in the numerical formulation because in the material point advection scheme (SULSKY *et al.* 1995) used here, state and history variables depend on material (Lagrangian ) coordinates rather than on spatial coordinates as in purely Eulerian formulations.

The initial overshoot and the subsequent drop of the parameters in figure 3 occur because the simulation was initiated from a perturbation of the non-convecting

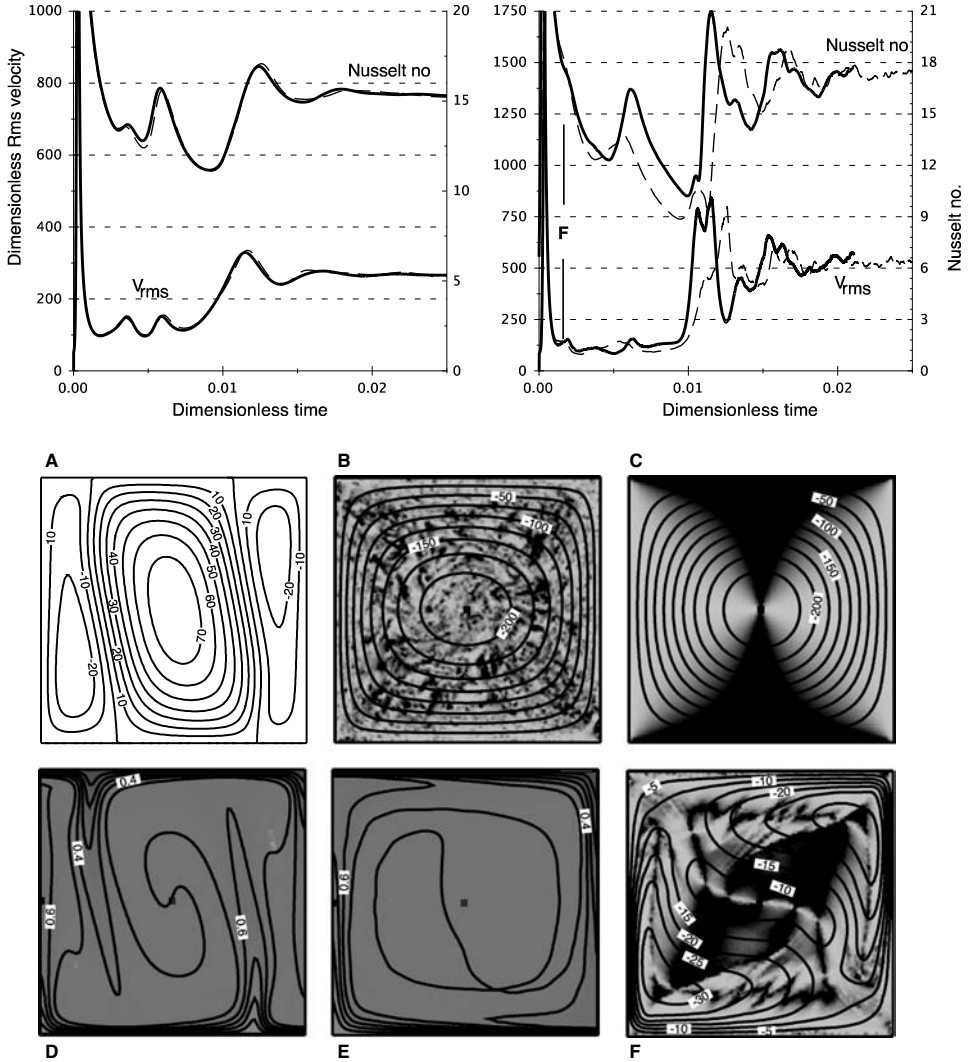


Figure 3

Time dependent convection. $Ra = 5.6 \times 10^5$. Time series plots of velocity and the Nusselt number isotropic convection (top left) and anisotropic convection, $\eta/\eta_S$ (top right). Dashed lines are the results of the $32 \times 32$ element simulations. The isotropic steady-state stream function (A) and temperature field (B) are compared with the anisotropic quasi-steady state (C,D, respectively). E, F show stream function and flow alignment for the anisotropic case at times 0 (E) and 0.0009 (F). Alignment is computed by $|\vec{n} \times \vec{v}|/|\vec{v}|$ with misalignment indicated by dark regions.

ground state which is far from the final equilibrium state. The system passes through a variety of configurations of hot plumes rising and cold plumes descending, until it finally settles to the steady states shown in figure 3. In the anisotropic case, this is a near-steady state in $V_{\text{rms}}$ velocity and Nusselt number, however the alignment

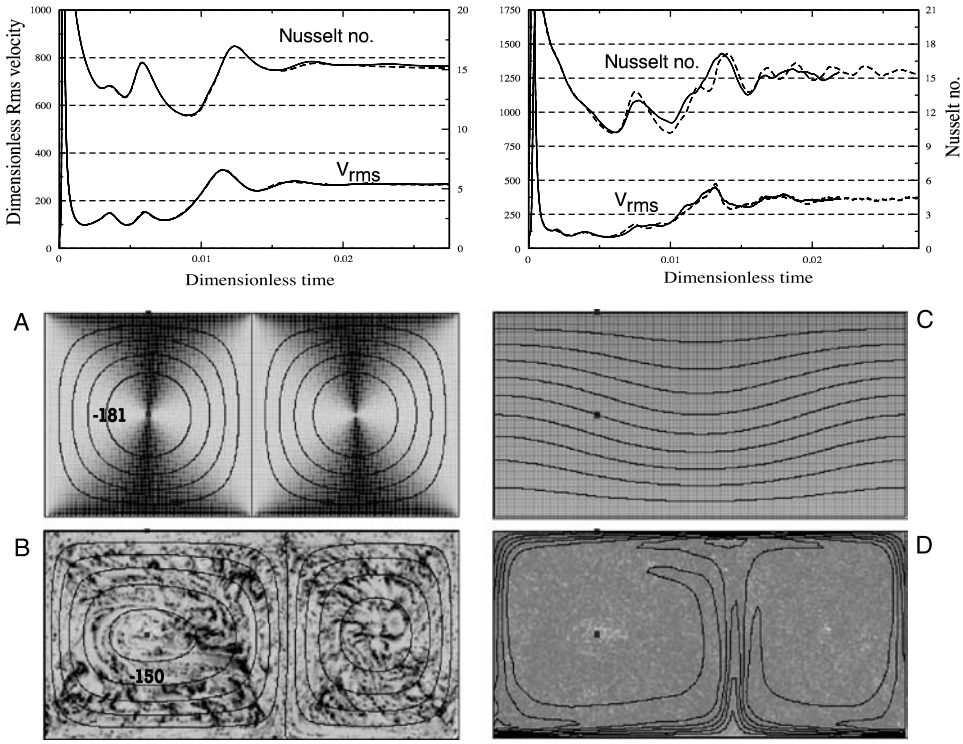


Figure 4
Time dependent convection in a $2 \times 1$ box. $Ra = 5.6 \times 10^5$. Time series plots of velocity and the Nusselt number isotropic convection (top left) and anisotropic convection, $\eta/\eta_S$ (top right). Dashed lines are the results of the coarse simulations, as in Figure 3. The initial state of alignment is shown in (a) and the initial thermal structure in (b), and after 4000 timesteps ($t = 0.04$) in (c) and (d).

patterns in the core of the convection cell continue to evolve slowly, producing small fluctuations. In this final state, the boundary layers are well aligned with the flow, but strain-rate gradients towards the stagnant core of the cell "freeze-in" a highly complicated pattern of orientation which is nearly isotropic at the resolution of the mesh. Note the additional resolution needed in the orthotropic case—although the pattern of evolution of the Nusselt number and $V_{\text{rms}}$ velocity is qualitatively similar, only the final state is quantitatively comparable.

## *Conclusion and Discussion*

We have presented a formulation for convection of anisotropic materials which incorporates time-dependent flow alignment. Alignment is modeled by introducting a Lagrangian evolution equation for the director. Lagrangian integration point finite element methods allow a simple and accurate implementation of this evolution

equation for arbitrarily large strain. The time-dependent aspect of flow alignment is important in interpreting the frozen-in flow directions which have been observed in the Australian lithosphere by DEBAYLE (1999) and DEBAYLE KENNETT (2000).

In the simple shear benchmarking against analytical solutions, we demonstrated the accuracy of this continuum approach for modeling emergent anisotropy. We then presented two case studies of convection in which anisotropy evolves with the flow to generate complex patterns of director alignment.

The convection simulations suggest that the anisotropic rheology produces a stabilizing effect on the convection pattern, and suppresses the tendency for the convection cells to break down during the early evolution of the system. An isotropic model of aspect ratio one passes through various stages of evolution before one dominant convection cell emerges. During this evolution, for a variety of initial perturbations, a long-lived pattern appears with small aspect ratio cells which generally break down to a single unit-aspect ratio cell to reach steady state. The orthotropic convection simulations in both box-sizes exhibit similar convective behavior but with a tendency for the orthotropic case to lock onto a longer wavelength pattern early. This tentative observation requires significantly more experiments to be done in wide aspect ratio boxes for clarification.

The thermal boundary layers are similar for orthotropic and isotropic cases. In the orthotropic simulation the director evolution follows the induced shear, and director alignment in rising plumes as well as director alignment in the boundary layers is visible in steady state. The well-aligned regions encircle a core of broadly disordered director orientation. As a consequence, we would expect that seismic anisotropy would be observed in boundary layers and other regions of high strain rate which persists.

This fits the observational evidence that deep mantle anisotropy is significantly smaller than in the shallow lithosphere (upper boundary layer), the 660 km discontinuity and the $D''$ layer (MONTAGNER and KENNETT (1996).

Considering the fact that we only use simple rheological models, there seems to be considerable promise in using this approach for more sophisticated modeling work which attempts to match and explain the observational evidence of seismic anisotropy.

The results presented represent research in progress. Future simulations will include the crystallographic slip model of section 3, include three-dimensionality and will focus on a comparison with the seismic observations of anisotropy in the lithosphere.

## REFERENCES

AKI, K. (1968), *Seismological Evidence for the Existence of Soft Thin Layers in the Upper Mantle under Japan*, J. Geophys. Res. *73*, 585–596.

BELYTSCHKO, T., LIU, W. K., and MORAN, B. *Nonlinear Finite Elements for Continua and Structures* (John Wiley and Sons, LTD, 2001) ISBN 0-471-98773-5.

CATHLES, L. M. *The Viscosity of the Earth's Mantle* (Princeton Univ. Press, Princeton, N. J. 1975)

CHRISTENSEN, U. C. (1984), *Convection with Pressure and Temperature Dependent Rheology*, Geophys. J. R. astr. Soc. *77*, 343–384.

CHRISTENSEN, U. C. (1987), *Some Geodynamical Effects of Anisotropic Viscosity*, Geophys. J. R. astr. Soc. *91*, 711–736.

DEBAYLE, E. (1999), *SV-wave Azimuthal Anisotropy in the Australian Upper Mantle: Preliminary Results from Automated Rayleigh Waveform Inversion*, Geophys. J. Int. *137*, 747–754.

DEBAYLE, E. and KENNETT, B. L. N. (2000), *Anisotropy in the Australian Upper Mantle from Love and Rayleigh Waveform Inversion*, Earth and Plan. Sci. Letters, *184*, 339–351.

DE GENNES, P. G. and PROST, J. *The Physics of Liquid Crystals*, (2nd edition, Clarendon Press, Oxford 1995).

FISCHER, K. M., PARMENTIER, E. M., STINE, A. R., and WOLF, E. R. (2000), *Modeling Anisotropy and Plate-driven Flow in the Tonga Subduction Zone Backarc,* J. Geophys. Res.-Solid Earth *105* (B7), 16,181–16,191.

FOUCH, M. J., FISCHER, K. M., PARMENTIER, E. M., WYSESSION, M. E., and CLARKE, T. J. (1997), *Shear Wave Splitting, Continental Roots, and Patterns of Mantle Flow*, MIT-Harvard Workshop on Continental Roots, Cambridge, MA.

HUGHES, T. J. R. (1984), *The Finite Element Method*, Prentice-Hall.

KARATO, S., WANG, Z., LIU, B., and FUJINO, K. (1995) *Plastic Deformation of Garnets: Systematics and Implication for the Rheology of the Mantle Transition Zone*, Earth Planet. Sci. Lett. *130*, 13–30.

KARATO, S.-I. (1998), *Seismic Anisotropy in the Deep Mantle, Boundary Layers and the Geometry of Mantle Convection*, Pure Appl. Geophys. *151*, 565–587.

MONTAGNER, J.-P., and KENNETT, B. L. N. (1996), *How to Reconcile Body-wave and Normal-mode Reference Earth Model*, Geophys. J. Int. *125*, 229–248.

MÜHLHAUS, H.-B., DUFOUR, F., MORESI, L., and HOBBS, B. (2002a) *A Director Theory for Viscoelastic Folding Instabilities in Multilayered Rock*, Int. J. Solids and Structures. *39*, 3675–3691.

MÜHLHAUS, H.-B., MORESI, L., HOBBS, B., and DUFOUR, F. (2002b), *Large Amplitude Folding in Finely Layered Viscoelastic Rock Structures*, Pure Appl. Geophys *159*, 2311–2333

NICOLAS, A., and CHRISTENSEN, N. I. (1987), *Formation of anisotropy in upper mantle peridotite*. In *Composition, Structure and Dynamics of the Lithosphere-Asthenosphere System* (Fuch, K. and, Froidevaux, C., (eds), Geodynamics Series *16*, 111–123.

SIMONS, F. J., VAN DER HILST, R. D., MONTAGNER, J.-P., and ZIELHUIS, A. (2002), *Multimode Rayleigh Wave Inversion for Heterogeneity and Azimuthal Anisotropy of the Australian Upper Mantle*, Geophysical J. Int., preprint: http://quake.mit.edu/ fjsimons/azimuthal.html, in press.

SPADA, G., YUEN, D. A., SABADINI, R., and BOSCHI, E. (1991), *Lower Mantle Viscosity Constrained by Seismicity around Deglaciated Regions*, Nature *351*, 53–55.

SULSKY, D., ZHOU, S.-J., and SCHREYER, H. L. (1995), *Application of a Particle-in-cell Method to Solid Mechanics*, Comput. Phys. Commun. *87*, 236–252.

TAKEUCHI, H., HAMANO, Y., and HASEGAWA, Y. (1968), *Rayleigh- and Lowe-wave Discrepancy and the Existence of Magma Pockets in the Upper Mantle*, J. Geophys. Res. *73*, 3349–3350.

YOUNG, T. E., GREEN, H. W., HOFMEISTER, A. M., and WALKER, D. (1993), *Infrared Spectroscopic Investigation of Hydroxil in beta-* $(Mg, Fe,)_2SiO_4$ *and coexisting olivine: Implications for mantle evolution and dynamics*, Phys. Chem. Minerals *19*, 409–422.

(Received September 27, 2002, revised February 28, 2003, accepted March 7, 2003)